



2-Phenyl-1,2,3-benzotriazole Ir(III) complexes with additional donor fragment for single-layer PhOLED devices

D. Tomkute-Luksiene^a, J. Keruckas^a, T. Malinauskas^a, J. Simokaitiene^a, V. Getautis^{a,**}, J.V. Grazulevicius^{a,*}, D. Volyniuk^b, V. Cherpak^b, P. Stakhira^{b,***}, V. Yashchuk^c, V. Kosach^c, G. Luka^d, J. Sidaravicius^e

^a Faculty of Chemical Technology, Kaunas University of Technology, 50254 Kaunas, Lithuania

^b Lviv Polytechnic National University, 79013 Lviv, Ukraine

^c Kyiv Taras Shevchenko National University, Faculty of Physics, 03680 Kyiv, Ukraine

^d Institute of Physics, Polish Academy of Sciences, 02-668 Warsaw, Poland

^e Department of Polygraphic Machines, Vilnius Gediminas Technical University, 03224 Vilnius, Lithuania

ARTICLE INFO

Article history:

Received 28 June 2012

Received in revised form

10 August 2012

Accepted 14 August 2012

Available online 23 August 2012

Keywords:

Iridium complexes

Triphenylamines

Carbazoles

Single-layer organic light emitting diode

Vacuum deposition

Phosphorescence

ABSTRACT

Phosphorescent bis-cyclometallated iridium (III) complexes based on 2-phenyl-1,2,3-benzotriazole with additional donor diphénylamine or carbazole moieties were synthesized, studied and tested as phosphorescent materials in the single-layer phosphorescent organic light emitting diodes. These single-layer devices were fabricated employing a simple technological approach, based upon the simultaneous vacuum deposition from one crucible of host material and the corresponding phosphorescent 1,2,3-triazole-based iridium complexes. Red and orange electrophosphorescent single-layer devices with current efficiencies of 5.3 cd/A and 6.8 cd/A respectively are reported. Results of the impedance spectroscopy suggest that the proposed method of formation of the working layer provides homogeneous distribution of molecular guest in the matrix of host.

© 2012 Elsevier Ltd. All rights reserved.

1. Introduction

Organic light-emitting diodes (OLEDs) have attracted a great deal of interest because of their potential applications in full-color flat-panel displays and lighting sources [1]. In recent years a lot of effort has been concentrated on the development of luminescent transition-metal complexes, particularly of the second- and third-row transition metals [2]. As a result of efficient spin-orbit coupling in these complexes, both singlet and triplet excitons can be harvested, and theoretically up to 100% internal quantum efficiencies can be attained.

In order to efficiently extract the electro-generated emissive excitons in typical electrophosphorescent device (PhOLED), various

functional layers for charge carrier injection, transport, blocking, as well as the confinement of exciton diffusion, are required [3]. Such sophisticated device configuration inevitably increases the manufacturing complexity and the production cost. It is therefore highly desirable to fabricate PhOLEDs with the simplified device structure. Particularly attractive goal is the single layer device, which can perform at the comparable efficiency as its multilayer counterparts. Efficient bi-layered devices consisting of emissive and buffer layers have been reported by several researchers [4–10]. However, the single-layer approach, adopting direct charge injection and transport onto the triplet dopants dispersed in an appropriate host matrix, is quite rare and only a very limited number of publications have been reported to date [11–17].

In the past few years various nitrogen-containing heterocycles such as quinolines, isoquinolines, quinazolines, and quinoxalines have been of special interest in accomplishing efficient orange and red phosphorescent emission from iridium complexes [18]. However, 1,2,3-triazoles have been overlooked and only recently few examples have been published [19–23]. The aim of the present

* Corresponding author. Tel.: +370 37 300193; fax: +370 37 456525.

** Corresponding author. Tel.: +370 37 300196; fax: +370 37 300152.

*** Corresponding author. Tel.: +380 50 2006563.

E-mail addresses: vytautas.getautis@ktu.lt (V. Getautis), juozas.grazulevicius@ktu.lt (J.V. Grazulevicius), stakhira@polynet.lviv.ua (P. Stakhira).

work was synthesis and characterization of orange and red-emitting 1,2,3-triazole-based iridium complexes bearing hole-transporting carbazolyl or diphenylamine moieties, and investigation of their suitability for the fabrication of the single-layer electrophosphorescent devices. The single-layer PhOLEDs were fabricated employing a simple technological approach, based upon the simultaneous vacuum deposition from one crucible of host material **CBM4** (Fig. 1a) and one of the phosphorescent emitting 1,2,3-triazole-based iridium complexes, red **IC1** (Fig. 1b) or orange **IC2** (Fig. 1c), at the ratio of 90% (**CBM4**): 10% (**IC1** or **IC2**).

2. Experimental details

2.1. Materials

All chemicals were purchased from Aldrich and used as received without further purification. The details of the synthesis of 5-amino-2-phenyl-1,2,3-benzotriazole are described in Ref. [24]. 1,1-Bis(4-(3',3''-dimethoxy)triphenylamino)cyclohexane (**CBM4**) was prepared by the earlier reported procedure [25].

2.2. General

The ^1H and ^{13}C NMR spectra were recorded on a Varian Unity Inova spectrometer (^1H -300 MHz, ^{13}C -75 MHz) at room temperature. The chemical shifts are expressed in ppm, downfield from tetramethylsilane (TMS), used as internal standard. The course of the reactions was monitored by TLC on ALUGRAM SIL G/JV254 plates and developed with UV light. Silica gel (grade 9385, 230–400 mesh, 60 Å, Aldrich) was used for column chromatography. Elemental analysis was performed with an Exeter Analytical CE-440 Elemental Analyzer. MS were recorded on an Agilent 110 (series MS with VL) apparatus. Cyclic voltammetry (CV) measurements were carried out by a three-electrode assembly cell from Bio-Logic SAS and a micro-AUTOLAB Type III potentiostat-galvanostat. The measurements were carried out with a glassy carbon electrode in dichloromethane solutions containing 0.1 M tetrabutylammonium hexafluorophosphate as electrolyte, Ag/AgNO₃ as the reference electrode and a Pt wire counter electrode. Thermogravimetric analysis (TGA) was performed with a Netzch STA 409 PC Luxx at a scan rate 10 K/min under a nitrogen flow. Differential scanning

calorimetry measurements were carried out on TA Instruments Q10 calorimeter at a heating rate of 10 °C/min in the nitrogen atmosphere. The glass transition temperatures (T_g) for the investigated compounds were determined during the second heating scan.

2.2.1. 5-Bis[(4-methylphenyl)amino]-2-phenyl-1,2,3-benzotriazole (**1**)

5-Amino-2-phenyl-1,2,3-benzotriazole (1.0 g, 4.76 mmol), 4-iodotoluene (2.59 g, 11.9 mmol), copper(I) iodide (0.033 g, 0.17 mmol), 2,2'-bipyridyl (0.027 g, 0.17 mmol) and potassium *tert*-butoxide (1.602 g, 14.28 mmol) were refluxed in 15 ml of dry toluene under argon atmosphere for 3 h. After termination of the reaction (TLC, *n*-hexane/acetone, 4:1 v/v) the mixture was filtered off and the solvent was evaporated. The residue was purified by column chromatography using *n*-hexane/acetone (24:1 v/v) as an eluent to afford **1** (0.78 g, 42%) as a yellow to orange solid. ^1H NMR (300 MHz, CDCl₃) δ , ppm: 8.29 (dd, $J = 8.7$ Hz, $J = 1.2$ Hz, 2H), 7.73 (dd, $J = 9.3$ Hz, $J = 0.9$ Hz, 1H), 7.51 (m, 2H), 7.39 (m, 1H), 7.31 (dd, $J = 2.1$ Hz, $J = 0.9$ Hz, 1H), 7.23 (dd, $J = 9.3$ Hz, $J = 2.1$ Hz, 1H), 7.14–7.03 (m, 8H), 2.34 (s, 6H). ^{13}C NMR (75 MHz, CDCl₃) δ , ppm: 147.90, 146.34, 145.17, 142.03, 140.48, 133.39, 130.20, 129.49, 128.50, 126.51, 125.22, 120.18, 118.46, 106.94. MS (APCI⁺, 20 V) m/z : 391 [M + H]⁺. Anal. Found: C, 79.87; H, 5.60; N, 14.53. C₂₆H₂₂N₄ requires C, 79.97; H, 5.68, N, 14.35%.

2.2.2. Iridium(III)-bis[5-bis[(4-methylphenyl)amino]-2-phenyl-1,2,3-benzotriazolato-*N,C2'*]acetyl-acetonate (**IC1**)

Iridium trichloride hydrate (0.47 g, 1.57 mmol) and **1** (1.3 g, 3.33 mmol) were dissolved in the mixture of 2-ethoxyethanol (20 ml) and water (2.5 ml). The mixture was refluxed under argon atmosphere for 20 h, and cooled down to ambient temperature. The formed crystals were filtered and washed with water and then ethanol. The product was dried under vacuum, and used in next step without further purification. The yield of the μ -chloride-bridged dimer was 1.18 g (37%).

The μ -chloride-bridged dimer (1.18 g, 0.586 mmol), 2,4-pentanedione (0.176 g, 1.75 mmol) and sodium carbonate (0.62 g, 5.85 mmol) were refluxed in 20 ml of degassed 2-ethoxyethanol under argon atmosphere for 2 h. After termination of the reaction (TLC, *n*-hexane/acetone, 4:1 v/v) the mixture was cooled down to ambient temperature and diluted with water (10 ml). The formed solid was isolated by filtration, washed with water and ethanol. The product was purified by column chromatography using *n*-hexane/acetone (24:1 and 23:2 v/v) as the eluent to obtain **IC1** (0.94 g, 78%) as red solid. ^1H NMR (300 MHz, CDCl₃) δ , ppm: 7.82–7.71 (m, 3H), 7.54–7.46 (m, 1H), 7.37–7.32 (m, 1H), 7.30–7.00 (m, 19H), 6.97–6.88 (m, 2H), 6.78–6.68 (m, 2H), 6.25–6.12 (m, 2H), 5.08 (s, 1H), 2.40–2.30 (m, 12H), 1.82 (s, 3H), 1.44 (s, 3H); ^{13}C NMR (75 MHz, CDCl₃) δ , ppm: 186.61, 186.08, 185.44, 149.58, 148.01, 145.58, 144.96, 144.90, 143.56, 142.89, 142.70, 140.63, 138.65, 134.59, 133.98, 133.73, 130.40, 130.30, 129.44, 128.14, 127.41, 125.69, 125.46, 122.43, 119.39, 115.65, 114.94, 106.54, 103.26, 103.21, 101.62, 28.36, 27.33, 27.12, 21.12; Anal. Found: C, 63.84; H, 4.55; N, 10.57. C₅₇H₄₉IrN₈O₂ requires C, 63.97; H, 4.61, N, 10.47%.

2.2.3. 2-Phenyl-5-iodo-1,2,3-benzotriazole (**2**)

Solution of 5-amino-2-phenyl-1,2,3-benzotriazole (8.4 g, 39.95 mmol) in acetic acid (150 ml) and hydrochloric acid (60 ml) was heated to 80 °C and the obtained brown suspension was then cooled down to 0 °C. Sodium nitrite (3.7 g, 53.62 mmol) in water (20 ml) was added slowly and the temperature was held at 0–5 °C throughout the addition. The resulting mixture was stirred for 45 min below 5 °C and then potassium iodide (9.6 g, 57.87 mmol) solution in water (40 ml) was added. The reaction mixture was warmed up to ambient temperature and then heated at 50 °C for 20 min. The mixture was cooled down to ambient temperature and

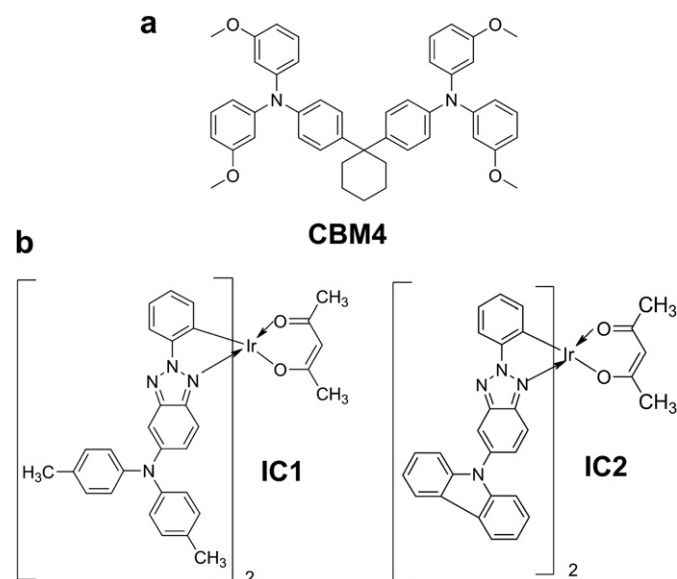


Fig. 1. Chemical structures of **CBM4**, **IC1**, **IC2**.

sodium metabisulfite was added until the red color disappeared. The solid was isolated by filtration, washed with aqueous sodium bicarbonate, water and finally hexane. The product was purified by column chromatography using *n*-hexane/acetone (24.5:0.5 v/v) as an eluent to yield 8.0 g (62%) of pale yellow solid. $^1\text{H NMR}$ (300 MHz, CDCl_3) δ , ppm: 8.36–8.28 (m, 3H), 7.71–7.60 (m, 2H), 7.58–7.42 (m, 3H). $^{13}\text{C NMR}$ (75 MHz, CDCl_3) δ , ppm: 145.56, 143.95, 140.07, 136.07, 129.59, 129.42, 127.57, 120.75, 119.96, 92.22; MS (APCI $^+$, 20 V) m/z : 322 $[\text{M} + \text{H}]^+$; Anal. Found: C, 44.99; H, 2.44; N, 12.97. $\text{C}_{12}\text{H}_8\text{IN}_3$ requires C, 44.88; H, 2.51, N, 13.09%.

2.2.4. 5-(9-Carbazolyl)-2-phenyl-1,2,3-benzotriazole (**3**)

Carbazole (1.15 g, 6.85 mmol), **2** (2.0 g, 6.23 mmol), copper (I)-tri(triphenylphosphine)bromide ($\text{Cu}(\text{PPh}_3)_3\text{Br}$) (0.5 g, 1.25 mmol) and cesium carbonate (3.04 g, 9.35 mmol) were refluxed in 30 ml of dimethyl sulfoxide under argon atmosphere for 8 h. After termination of the reaction (TLC, *n*-hexane/acetone, 22:3 v/v) the mixture was treated with dichloromethane and water. The organic layer was dried over anhydrous sodium sulfate, filtered and solvents were evaporated. The obtained residue was purified by column chromatography using *n*-hexane/acetone (24:1 v/v) as an eluent to obtain **3** (1.45 g, 65%) as yellow solid. $^1\text{H NMR}$ (300 MHz, CDCl_3) δ , ppm: 8.46–8.40 (m, 2H), 8.22–8.13 (m, 4H), 7.70–7.58 (m, 3H), 7.55–7.42 (m, 5H), 7.38–7.27 (m, 2H). $^{13}\text{C NMR}$ (75 MHz, CDCl_3) δ , ppm: 145.64, 144.22, 141.00, 140.43, 136.77, 129.76, 129.52, 127.57, 127.51, 126.35, 123.78, 120.86, 120.63, 120.51, 120.24, 116.18, 110.02; MS (APCI $^+$, 20 V) m/z : 361 $[\text{M} + \text{H}]^+$; Anal. Found: C, 79.95; H, 4.40; N, 15.65. $\text{C}_{24}\text{H}_{16}\text{N}_4$ requires C, 79.88; H, 4.47, N, 15.54%.

2.2.5. Iridium(III)-bis[5-(9-carbazolyl)-2-phenyl-1,2,3-benzotriazolato-*N,C2'*]acetyl-acetonate (**IC2**)

Iridium trichloride hydrate (0.316 g, 1.06 mmol) and **3** (0.8 g, 2.2 mmol) were dissolved in the mixture of 2-ethoxyethanol (25 ml) and water (3 ml). The mixture was refluxed under argon atmosphere for 22 h, and cooled down to ambient temperature. The formed crystals were filtered and washed with water and then

hexane. The product was dried under vacuum, and used in next step without further purification. The yield of the μ -chloride-bridged dimer was 0.88 g (44%).

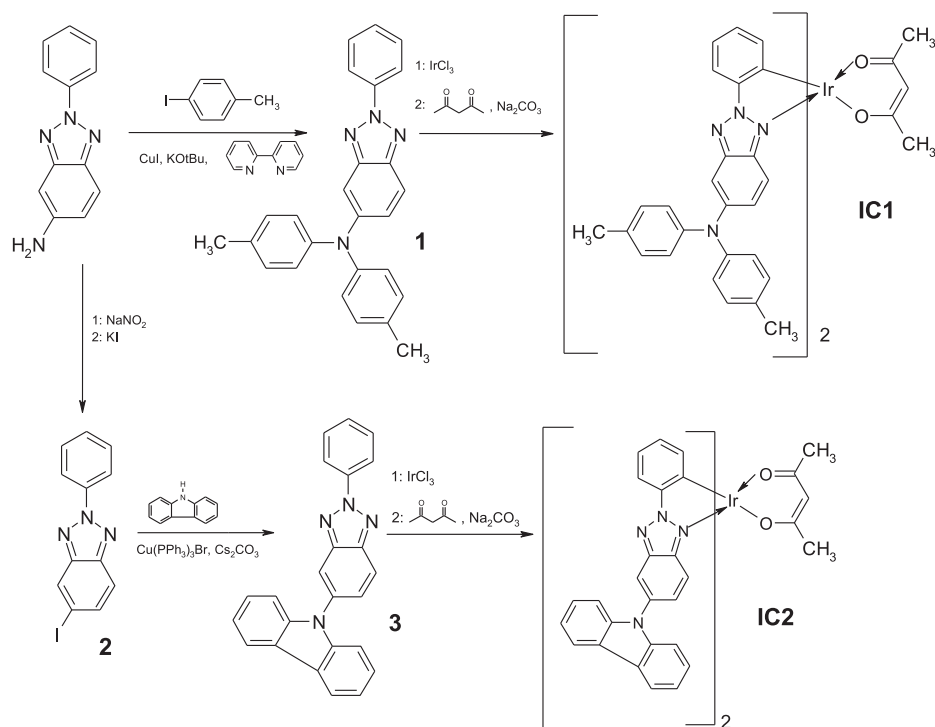
The μ -chloride-bridged dimer (0.88 g, 0.46 mmol), 2,4-pentanedione (0.14 g, 1.40 mmol) and sodium carbonate (0.49 g, 4.62 mmol) were refluxed in 20 ml of degassed 2-ethoxyethanol under argon atmosphere for 3 h. After termination of the reaction (TLC, *n*-hexane/acetone, 4:1 v/v) mixture was cooled down to ambient temperature and diluted with water (10 ml). The formed solids were isolated by filtration, washed with water and ethanol. The product was purified by column chromatography using *n*-hexane/acetone (24:1 and 23:2 v/v) as the eluent to obtain **IC2** (0.61 g, 65%) as orange solid. $^1\text{H NMR}$ (300 MHz, CDCl_3) δ , ppm: 8.25–8.12 (m, 5H), 8.07–7.95 (m, 4H), 7.90–7.82 (m, 1H), 7.77–7.30 (m, 14H), 7.12–6.96 (m, 2H), 6.90–6.75 (m, 2H), 6.37–6.25 (m, 2H), 5.48 (s, 1H), 1.95 (s, 3H), 1.50 (s, 3H); $^{13}\text{C NMR}$ (75 MHz, CDCl_3) δ , ppm: 187.11, 186.65, 186.49, 144.75, 144.71, 142.83, 142.79, 142.55, 141.19, 140.87, 140.54, 138.97, 137.00, 136.96, 134.92, 134.82, 130.24, 130.19, 130.13, 129.55, 129.24, 126.96, 126.89, 126.45, 124.11, 123.95, 123.07, 122.99, 122.95, 122.88, 121.16, 120.94, 120.79, 120.72, 120.68, 116.93, 116.90, 116.81, 116.69, 111.85, 110.05, 101.92, 68.66, 28.48, 22.22; Anal. Found: C, 63.10; H, 3.80; N, 10.96. $\text{C}_{53}\text{H}_{37}\text{IrN}_8\text{O}_2$ requires C, 63.02; H, 3.69, N, 11.09%.

2.3. Fabrication and characterization of the films and devices

The electroluminescent devices ITO/**CBM4:IC1**(26 nm)/Ca(40 nm)/Al(200 nm) (**A**) and ITO/**CBM4:IC2**(26 nm)/Ca(40 nm)/Al(200 nm) (**B**) were fabricated by means of vacuum co-deposition of **CBM4** and **IC1** (**IC2**) from one source boat (at the ratio of 90% (**CBM4**): 10% (**IC1** or **IC2**)) onto ITO coated glass substrate under vacuum of 10^{-5} Torr.

The thickness of the layers of **CBM4:IC1** and **CBM4:IC2** was measured by NanoCalc 2000 Reflectometry System. The active area of the obtained devices **A** and **B** was $3 \times 2 \text{ mm}^2$.

For the measurements of photoluminescence (PL) and absorption spectra of **CBM4**, **IC1**, **IC2**, **CBM4:IC1** and **CBM4:IC2** the films were



Scheme 1. Synthesis of iridium complexes **IC1**, **IC2**.

vacuum deposited on quartz substrates. UV spectra were recorded with Cary 5000 UV–VIS–NIR and Specord UV–Vis spectrometers. For the measurements of photoluminescence spectra of **CBM4** the films were casted from tetrahydrofuran (THF) solution on quartz substrates. Low-temperature (77 K) photoluminescence measurements were performed using the cryostat Optistat (Oxford Instruments).

The current density–voltage–luminance (J – V – L) characteristics and electroluminescence (EL) spectra were recorded using a Programmable Test Power LED300E, spectrometer HAAS-2000 and integrated sphere ($d = 0.3$ m).

Impedance spectroscopy was employed for the characterization of the conductive properties of devices **A** and **B**. Experiments were performed in the frequency range of $10^1 \div 10^6$ Hz at constant bias voltage of 0 V, 1.0 V, 3.0 V and 5 V using “AUTOLAB” spectrometer (Eco Chemie, The Netherlands) and FRA-2 and GPES software. Frequency dependencies of complex resistivity Z were analyzed by graphic–analytical method using ZView 2.3 (Scribner Associates) package. Approximation inaccuracy was found not to exceed 2%.

3. Results and discussion

3.1. Synthesis and thermal characterization

Synthesis of the iridium complexes **IC1** and **IC2** containing 2-phenyl-1,2,3-benzotriazole moieties was carried out by a synthetic route given in Scheme 1. 2-Phenyl-5-iodo-1,2,3-benzotriazole (**2**) was synthesized using a classical Sandmeyer reaction, while ligands 5-bis[(4-methylphenyl)-amino]-2-phenyl-1,2,3-benzotriazole (**1**) and 5-carbazolyl-2-phenyl-1,2,3-benzotriazole (**3**) were prepared using modified Ullmann-type reactions. Nonoyama reaction of the corresponding ligands and $\text{IrCl}_3 \cdot n\text{H}_2\text{O}$ in a mixed solvent system of 2-ethoxyethanol and water gave the intermediate cyclometalated μ -chloride-bridged Ir(III) dimer. Subsequently, chloride of μ -chloride-bridged Ir(III) dimer was substituted by the acetylacetonate ligand in the presence of potassium carbonate base in a thoroughly degassed 2-ethoxyethanol at 135 °C.

Thermal behavior of the complexes **IC1**, **IC2** was explored by DSC and TGA methods. Melting points (T_m), glass transition temperatures (T_g) and 5% mass loss temperatures (T_{dec}) were established, and the data are summarized in Table 1.

Both complexes are amorphous materials with high glass transition temperatures (Fig. 2). Replacement of the relatively flexible diphenylamine moiety with the rigid carbazole unit results in the increase of T_g by 31 °C. TGA performed under nitrogen with the heating rate of 10 K/min revealed good thermal stability of the synthesized compounds. Their thermal degradation starts above 370 °C.

3.2. Optical, photophysical, and electrochemical properties

Fig. 3 shows absorption and photoluminescence spectra of the **CBM4** films prepared by casting from THF solutions at room temperature.

Table 1
Thermal characteristics of **CBM4** and **IC1**, **IC2**.

Compound	T_g , (°C) ^a	T_m , (°C) ^b	T_{dec} , (°C) ^c
IC1	181	–	383
IC2	212	–	370
CBM4	48	123	454

^a Determined by DSC: scan rate, 10 K/min; N_2 atmosphere; second run.

^b Melting point was only detected during the first heating; the compound vitrified on cooling to room temperature with 10 K/min.

^c Onset of decomposition determined by TGA: heating rate, 10 K/min; N_2 atmosphere.

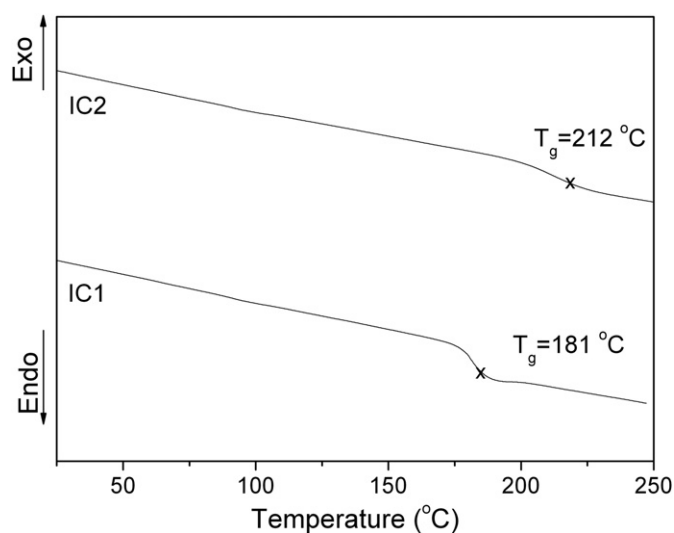


Fig. 2. DSC second heating curves for **IC1** and **IC2** (heating rate 10 K/min).

Absorption spectra of spin-coated films (Fig. 3a) can be characterized by non-structured absorption band at 310 nm due to π – π^* transitions. The short-wave PL maximum of **CBM4** films (at 300 K) is observed at 366 nm with corresponding Stokes shift of 56 nm. In order to evaluate the energy of the first triplet state of the

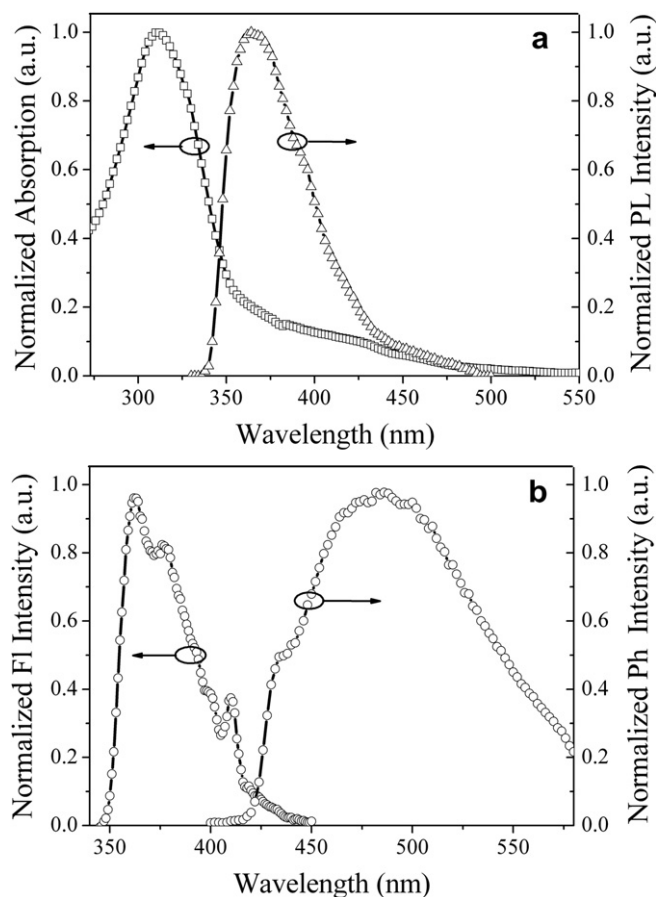


Fig. 3. Normalized absorption and photoluminescence spectra of the **CBM4** films prepared by casting from THF solutions at room temperature (a); photoluminescence and phosphorescence spectra of the **CBM4** films at 77 K (b).

molecule, low-temperature (77 K) emission measurements were performed. Fluorescence spectrum of the film of **CBM4** at 77 K is more structured compared to the room temperature one (Fig. 3b). Phosphorescence spectrum of the **CBM4** film at 77 K has four main emission peaks at 435 nm, 463 nm, 481 nm and 500 nm.

Fig. 4a and b shows normalized absorption and phosphorescence spectra of the vacuum deposited films of **IC1**, **IC2** at 300 K and 77 K, and of dilute solutions of **IC1** and **IC2** in toluene at 300 K. The absorption spectrum of the vacuum deposited film of **IC1** corresponds to the absorption spectrum of its dilute toluene solution and has the maximum around 300 nm, which is due to intra-ligand $\pi-\pi^*$ transitions, and the peak at 450 nm which can be assigned to metal-to-ligand charge transfer (MLCT) [26].

The character of the absorption spectrum of the film of **IC2** corresponds to that of toluene solution and peaks at around 340 nm are due to the presence of carbazole moieties [24]. In a lower energy region from 380 to 460 nm (Fig. 4b) weak and broad absorption bands with the corresponding shoulders are observed, which can be attributed to spin-allowed and spin-forbidden MLCT transitions of the Ir(III) complexes [26]. The wavelengths of absorption and phosphorescence maxima are summarized in Tables 2 and 3.

The PL spectra of the iridium complexes **IC1** and **IC2** are little changed going from solution to the film, although low-temperature (77 K) emission spectra are somewhat more structured. Due to the presence of stronger electron donor diphenylamine, **IC1** has a red shifted emission maximum, compared to that of **IC2**, ~610 nm and ~570 nm accordingly. However, due to less rigid structure of **IC1** and narrower band gap, more energy is lost in nonradiative pathways and overall quantum yield in toluene solutions is lower (41% for **IC2** and 21% for **IC1**).

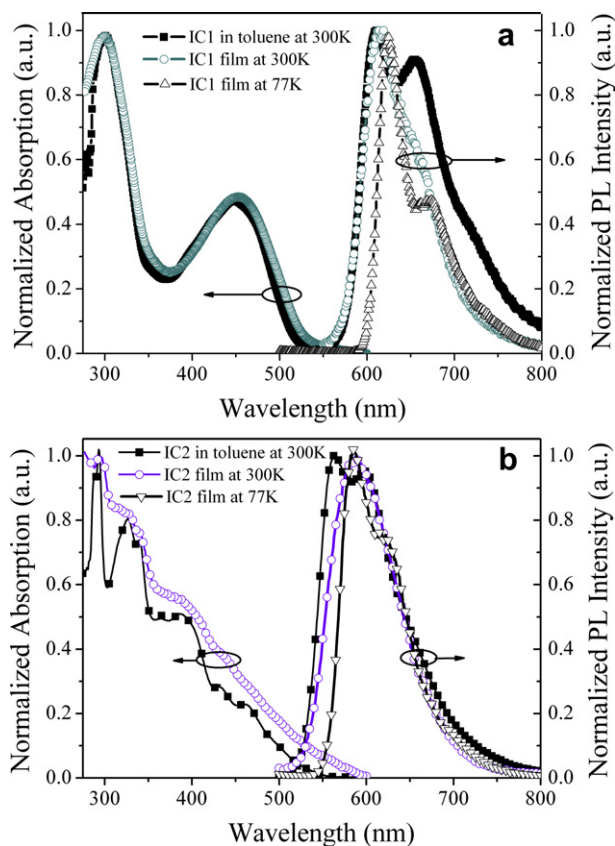


Fig. 4. Normalized absorption and phosphorescence spectra of the toluene solutions (10^{-5} M) and solid films of **IC1** (a), **IC2** (b) at 300 K and 77 K.

Table 2

Optical and photophysical characteristics of the toluene solutions of **IC1**, **IC2**.

	$\lambda_{\text{max}}^{\text{ab}}$ (nm)	$\text{Log } \epsilon$, ($\text{M}^{-1} \times \text{cm}^{-1}$)	$\lambda_{\text{ph}}^{\text{max}}$ (nm)	η , (%)
IC1	300, 450	4.76, 4.39	611, 654	21
IC2	292, 326, 340, 393, 433, 460	4.67, 4.54, 4.49, 4.34, 4.09, 3.99	564, 597	41

Table 3

Photophysical characteristics of the films of **IC1**, **IC2**, and films of **CBM4**, **CBM4:IC1**, **CBM4:IC2**.

	$\lambda_{\text{max}}^{\text{a,b}}$ (nm)	$\lambda_{\text{FL}}^{\text{max}}$ (nm)	$\lambda_{\text{Ph}}^{\text{max}}$ (nm)
IC1 ^a	300, 453	–	613
IC2 ^a	294, 314, 326, 340, 388, 437	–	588
CBM4 ^b	313	367	435, 463, 481, 500
CBM4:IC1 ^a	366, 451	–	613
CBM4:IC2 ^a	312, 385	–	566, 591

^a Vacuum deposited films.

^b Films deposited from THF solution.

The absorption spectrum of the film of the host-guest system **CBM4:IC1** (Fig. 5) is characterized by two bands i.e. the short wavelength band with the maximum at 369 nm and long-wavelength band peaking at 420–520 nm. The latter is apparently due to MLCT. The absorption spectrum of the film of the host-guest system **CBM4:IC2** is characterized by two bands i.e. by the short wavelength band peaking at 314 nm characteristic to **CBM4** and by the long-wavelength band peaking at 360–460 nm that could be assigned to MLCT complex.

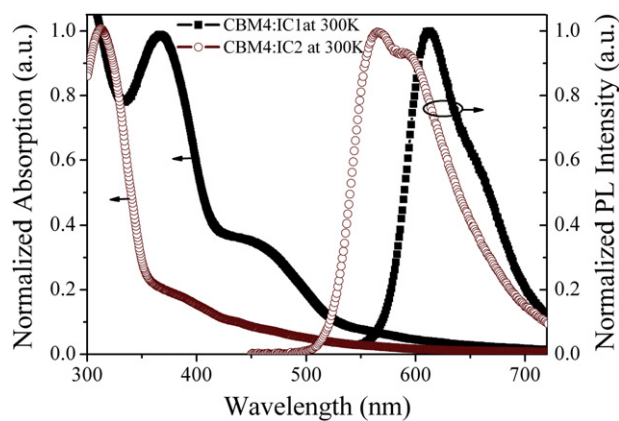


Fig. 5. Normalized absorption and PL spectra of the solid films **CBM4:IC1** and **CBM4:IC2** at 300 K.

Table 4

E_{HOMO} , E_{LUMO} , I_{p} , band gap and triplet energies for **CBM4**, **IC1** and **IC2**.^a

Compound	$E_{1/2, \text{red}}$ vs Fc, (V)	$E_{1/2, \text{ox}}$ vs Fc, (V)	E_{HOMO} , (eV) ^c	E_{LUMO} , (eV)	E_{g} , (eV)	E_{T} , (eV) ^f
IC1	–2.25	0.50	–5.30	–2.55	2.75	2.02
IC2	–2.07	0.76	–5.56	–2.73	2.83	2.11
CBM4	–	0.37 ^b	–5.17	–1.62 ^d	3.55 ^e	2.85

^a The CV measurements were carried out at a glassy carbon electrode in dichloromethane solutions containing 0.1 M tetrabutylammonium hexafluorophosphate as electrolyte and Ag/AgNO₃ as the reference electrode. Each measurement was calibrated with ferrocene (Fc).

^b Oxidation not reversible, E_{onset} calculated.

^c E_{HOMO} , $E_{\text{LUMO}} = -(4.8 + E_{1/2} \text{ vs Fc})$.

^d $E_{\text{LUMO}} = E_{\text{HOMO}} - E_{\text{g}}^{\text{opt}}$.

^e The optical band gaps $E_{\text{g}}^{\text{opt}}$ estimated from the edge of electronic absorption spectra.

^f E_{T} triplet energy measured in films at 77 K.

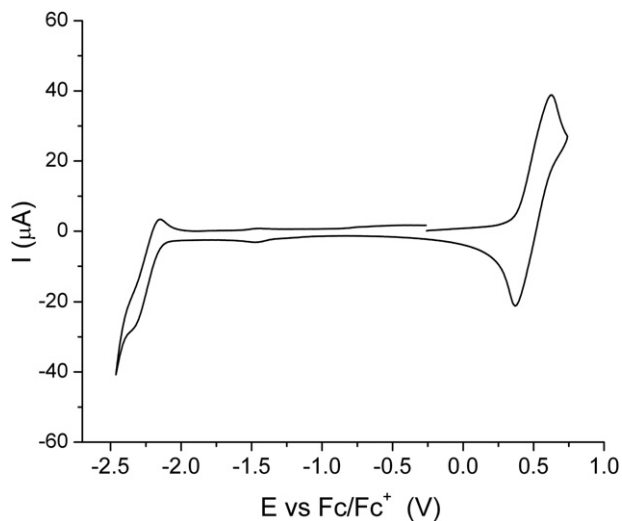


Fig. 6. First oxidation and reduction waves of **IC1** (scan rate = 200 mV s^{-1}) in argon-purged dichloromethane solution.

PL spectrum of the film of the mixture **CBM4:IC2** (Fig. 5) has maxima at ca. 562 and 600 nm and is similar to the PL spectrum of the film and toluene solution of **IC2** (Fig. 4a). The similar picture is observed for the film of **CBM4:IC1**, but long-wavelength luminescence band is not clearly expressed. No **CBM4** emission was observed in the PL spectra of the films of the host-guest systems.

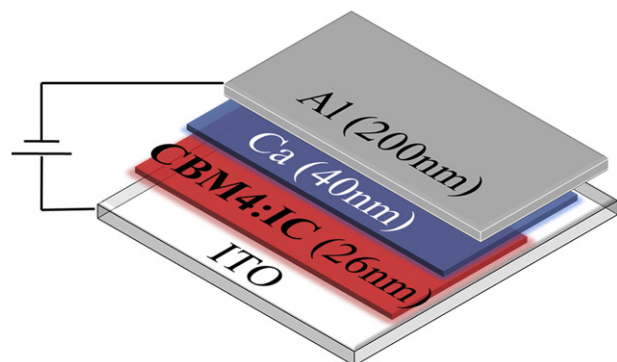


Fig. 7. The general structure of the single-layer PhOLED.

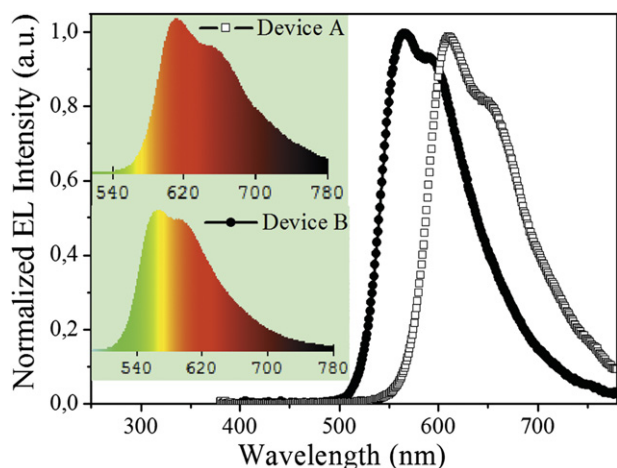


Fig. 8. Electroluminescence spectra of the devices A and B.

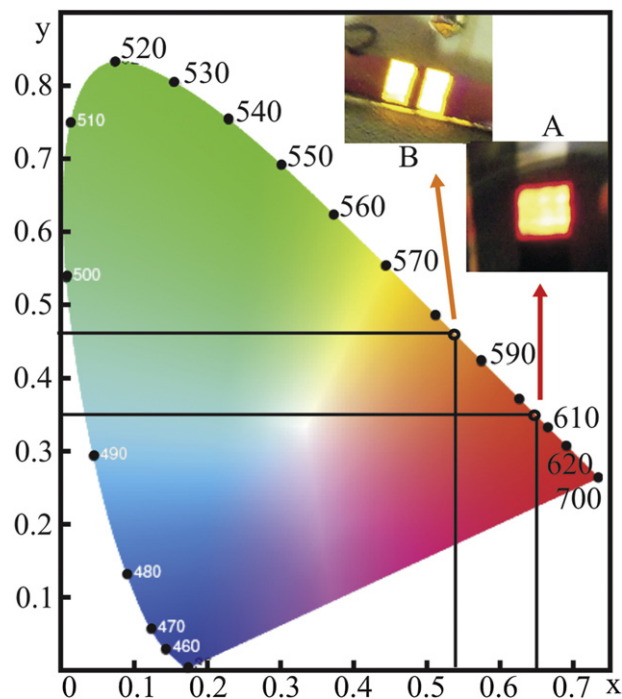


Fig. 9. CIE 1931 chromaticity diagram and photos of the devices A and B.

PL spectrum of **CBM4** partially overlaps with absorption band of **IC1** (Fig. 3b and Fig. 4a) and fully overlaps with the MLCT absorption band of **IC2** (Fig. 4b). Thus, efficient electronic excitation energy transfer is expected to take place from **CBM4** to **IC1** and **IC2** [27].

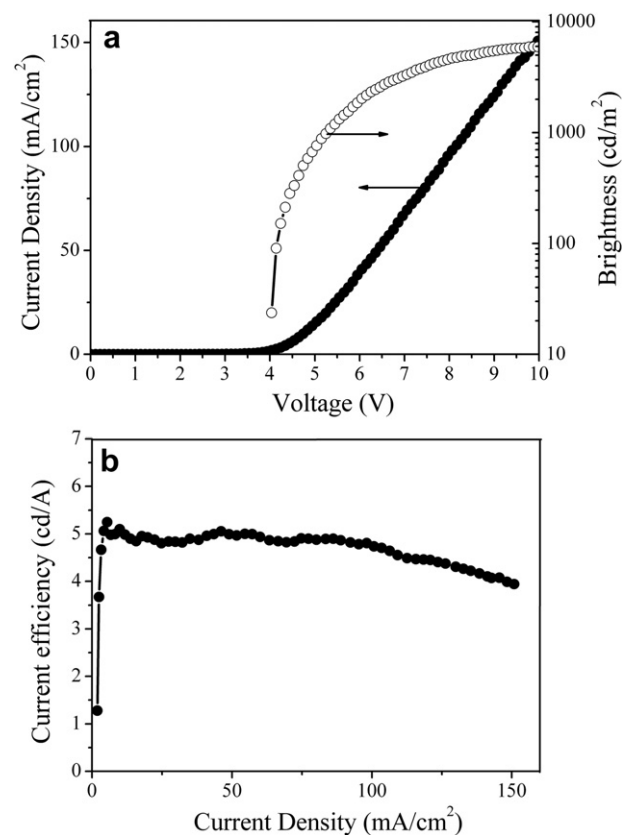


Fig. 10. Current density–voltage and luminance–voltage characteristics (a) and current efficiency–current density characteristics (b) for electroluminescent device A.

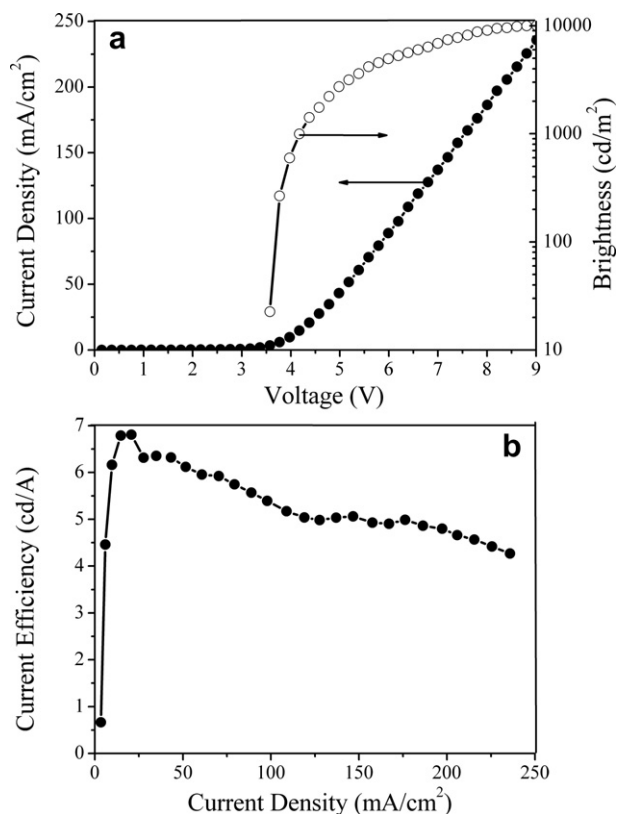


Fig. 11. Current density–voltage and luminance–voltage characteristics (a) and current efficiency–current density characteristics (b) for electroluminescent device B.

This observation indicates that PL emission originates from the triplet excited states of the **IC1** and **IC2** complexes [28] and suggests that energy transfer from **CBM4** host to Ir(III) complexes is efficient.

Moreover, a sufficiently higher triplet level of the **CBM4** (ca. 2.8 eV, Fig. 3b) allows efficient exciton confinement on the guest **IC1** and **IC2** complexes. The triplet energy of **CBM4** is higher than the T1-energy of **IC1** and **IC2** by more than 0.8 eV and 0.7 eV respectively (Table 4).

To elucidate the energetic conditions for energy and electron transfer in dilute solutions, the E_{HOMO} and E_{LUMO} values were also determined using cyclic voltammetry (CV) (Table 4). The cyclic voltammograms of the synthesized compounds in dichloromethane show quasi-reversible oxidation and reduction couples (Fig. 6).

IC1, with diphenylamine moiety, exhibits the first oxidation wave half-wave potential corresponding to 0.5 V vs Fc, which results in a E_{HOMO} value of -5.30 eV (on the basis of the E_{HOMO} energy level of ferrocene as 4.8 eV) and the first reduction half-wave potential of -2.25 V vs Fc, resulting in $E_{\text{LUMO}} = -2.55$ eV. Substitution of the diphenylamine moiety with that of carbazole in **IC2** results in the decrease of both E_{HOMO} and E_{LUMO} values, as well as in the slight increase of band gap E_g . These changes in energy levels of **IC2** result in the blue shift of the PL emission maxima by ~ 50 nm (from 611 nm for **IC1** to 564 nm for **IC2**).

3.3. Characterization of PhOLED

Two types of single-layer electroluminescent devices of the configurations ITO/**CBM4:IC1**(26 nm)/Ca (40 nm)/Al (200 nm) (**A**) and ITO/**CBM4:IC2**(26 nm)/Ca (40 nm)/Al (200 nm) (**B**) were fabricated by means of vacuum co-deposition of **CBM4** and **IC1** or **IC2** from one source boat (at the ratio of 90% (**CBM4**): 10% (**IC1** or **IC2**)) onto ITO coated glass substrate (Fig. 7). Electroluminescence maxima are observed at 610 nm and 650 nm for the device A and at 562 and 600 nm for the device B (Fig. 8). The shapes of the spectra of electroluminescence of the devices A and B are similar to those of PL spectra of the solid films of the mixtures of **CBM4:IC1** and **CBM4:IC2** respectively (Fig. 5). This observation confirms the electrophosphorescent emitting nature of the devices.

Commission Internationale de l'Eclairage (CIE 1931) chromaticity coordinates (x, y) of the devices A and B were found to be (0.44, 0.53) and (0.28, 0.56) corresponding to the red and orange color respectively (Fig. 9, Table 4).

The device A reaches the current efficiency of ca. 5.0 cd/A (Fig. 10b) and this value is almost independent on the current density in the range from 20 to 100 mA/cm².

Lower turn on voltage value (Table 5) of the device B can apparently be explained by the better match of energy levels of the host and guest and of the work function of cathode (Fig. 12). The difference in brightness of the devices A and B is apparently due to the higher sensitivity of eye to the luminescence spectral range of the device B.

Energy-band diagrams of OLEDs A and B are shown in Fig. 12a and b. E_{HOMO} and E_{LUMO} values of the iridium complexes were determined using cyclic voltammetry (CV). The E_{LUMO} of the **CBM4** was calculated from its optical band gap (E_g^{opt}) and E_{HOMO} obtained from the CV measurements ($E_{\text{LUMO}} = E_{\text{HOMO}} - E_g^{\text{opt}}$).

3.4. Characterization of the devices A and B by impedance spectroscopy

Fig. 13a,b show experimental data of the impedance Z of the device, measured at three different bias voltages, i.e. 0 V, 1 V, 3 V and 5 V (symbols correspond to experimental data and the solid lines represent the fitting data). The dependence is represented by one semicircle, thus making possible to model the current flow in the structure using the equivalent circuit characteristic of the diode structure, consisting of one R1C1 circuits in serial with R_s (Fig. 13c).

The data presented in Tables 5 and 6 show that C1 remains rather constant versus bias voltage for the frequency range measured and R1 drops significantly as the bias voltage increases, especially at voltages higher than the threshold voltage of the structures (Figs. 10 and 11). The elements C1 and R1 represent bulk components and are determined by the electrical properties of the host-guest organic electroluminescent layers (**CBM4:IC1** and **CBM4:IC2**) [29]. R_s corresponds to overall contact resistance of the structures.

As the applied bias increases the resonance frequency ω_p shifts towards the higher frequency indicating a decrease in relaxation time (Tables 6 and 7). This observation can be explained by the decrease in the resistance of the bulk as the number of injected charge carriers increases [30].

Table 5
EL characteristics of the devices A and B.

Devices	V_{on} (V)	L_{max} (cd/m ²)	LE_{max} (cd/A)	EQE_{max} (%)	$\lambda_{\text{max}}^{\text{el}}$ (nm)	CIE 1931 XYZ coordinates, (x, y)	CIE 1960 UCS coordinates, (u, v)	T_c (K)
A	4.0	5945	5.3	2.29	610, 652	(0.65, 0.35)	(0.44, 0.53)	2436
B	3.6	10,060	6.8	1.45	566, 592	(0.53, 0.47)	(0.28, 0.56)	1054

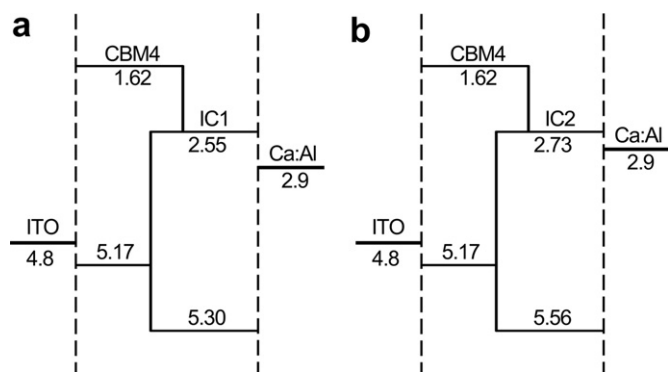


Fig. 12. Energy-band diagrams of the devices A(a) and B(b).

From the good agreement between the experimental data and the model for all the applied bias voltages and for all the frequency range, one can conclude about the absence of additional potential barriers throughout the structures that indicate effective energy transfer from the host to guest and the minimum of energy barrier between the electrodes and organic materials (Fig. 12).

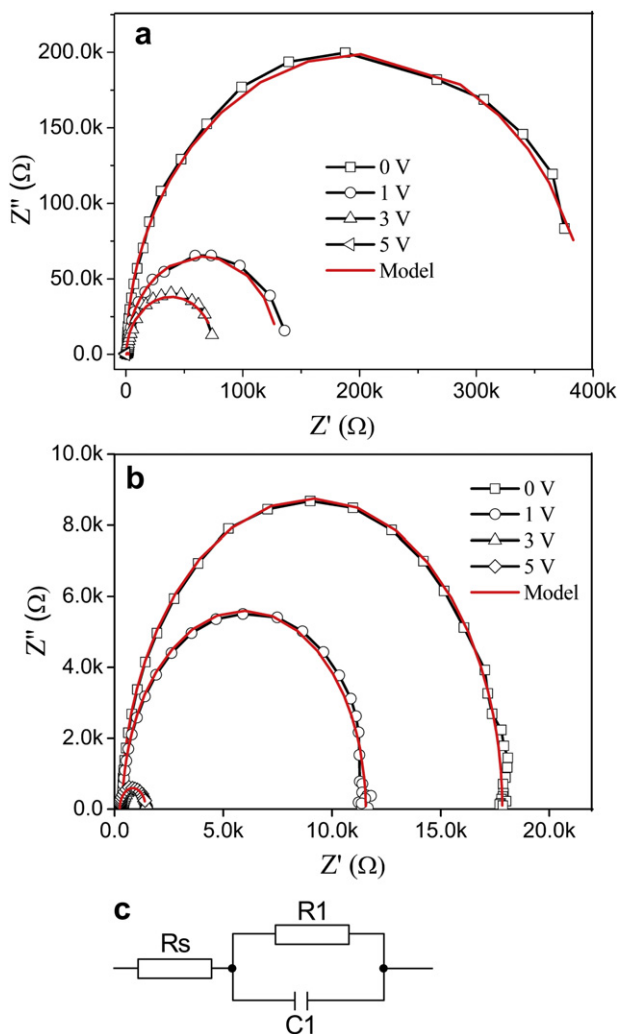


Fig. 13. Impedance spectra of the device A (a), B (b) and equivalent circuits (c).

Table 6

Fitting parameters of impedance data for device A at various bias voltages.

Bias voltage, (V)	Value element				
	Serial resistor R1, (Ω)	Parallel resistor R2, (k Ω)	Parallel capacitor C1, (nF)	Peak frequency, (kHz)	Dielectric relaxation time, (μ s)
0	470.2	397.5	6.3	2	500
1	471.1	129.7	6.2	3.2	312.5
3	470	76.2	6.2	5	200
5	448.6	1.9	4.6	40	25

Table 7

Fitting parameters of impedance data for device B at various bias voltages.

Bias voltage, (V)	Value element				
	Serial resistor R1, (Ω)	Parallel resistor R2, (k Ω)	Parallel capacitor C1, (nF)	Peak frequency, (kHz)	Dielectric relaxation time, (μ s)
0	344	17.5	5.7	10	100
1	361	11.2	5.6	12.6	79
3	342	1.2	5.2	50.1	20
5	238.5	1.2	5.2	63	16

4. Conclusions

Phosphorescent bis-cyclometallated iridium(III) complexes based on the 2-phenyl-1,2,3-benzotriazole with additional donoric units were synthesized. The isolated amorphous compounds were found to express good solubility in common organic solvents, and high glass transition temperatures. The obtained iridium complexes were found to exhibit red and orange phosphorescence at 610 and 570 nm respectively with the CIE chromaticity coordinates of (0.65, 0.35) for **IC1** and (0.53, 0.47) for **IC2**. Stronger diphenylamine donoric unit in **IC1** has more influence on the energy levels of the molecule, which results in a bathochromic shift of the PL emission maxima compared with carbazole-containing **IC2**.

It was shown that the phosphorescence of the **CBM4** films occurs in the region of 2.5–2.8 eV. According to evaluation the position of triplet level of **CBM4** is by more than 0.7 eV higher than the first excited triplet states of **IC1** and **IC2** and allows efficient exciton confinement on the guest complexes.

Single-layer PhOLEDs were fabricated employing a simple technological approach, based upon the simultaneous vacuum deposition from one crucible of host material **CBM4** and a phosphorescent 1,2,3-triazole-based iridium complex. The maximum brightness of the obtained PhOLEDs is about 6000 and 10,000 cd/m² with current efficiency 5.3 cd/A and 6.8 cd/A for the devices with **IC1** and **IC2** respectively. These characteristics are quite high, taking into the account the absence of any additional injection and transport layers in the constructed PhOLEDs.

The results of impedance spectroscopy suggest that the proposed method of formation of emitting layer provides homogeneous distribution of molecular guest in the matrix of host and the PhOLED is characterized by low energy barrier between the electrodes and host-guest layer.

Acknowledgments

The support from the programme of collaboration in the field of science and technologies between Lithuania and Ukraine is gratefully acknowledged (project No TAP LU 01/2012). This research was funded by the European Social Fund under the Global Grant measure (VP1-3.1-ŠMM-07-K 01-078). We would also want to thank Dr. Karolis Kazlauskas (Vilnius University, Lithuania) for photoluminescence quantum yield measurements.

References

- [1] Pfeiffer M, Forrest SR, Leo K, Thomson ME. Electrophosphorescent p–i–n organic light-emitting devices for very-high-efficiency flat-panel displays. *Adv Mater* 2002;14:1633–6.
- [2] (a) Yersin H, Strasser J. Triplets in metal–organic compounds. *Chemical tunability of relaxation dynamics. Coord Chem Rev* 2000;208:331–64; (b) Köhler A, Wilson JS, Friend RH. Fluorescence and phosphorescence in organic materials. *Adv Mater* 2002;14:701–7; (c) Nozaki K, Takamori K, Nakatsugawa Y, Ohno T. Theoretical studies of phosphorescence spectra of tris(2,2′-bipyridine) transition metal compounds. *Inorg Chem* 2006;45:6161–78; (d) Lowry MS, Bernhard S. Synthetically tailored excited states: phosphorescent, cyclometalated iridium(III) complexes and their applications. *Chem Eur J* 2006;12:7970–7; (e) Chou PT, Chi Y. Osmium- and ruthenium-based phosphorescent materials: design, photophysics, and utilization in OLED fabrication. *Eur J Inorg Chem* 2006:3319–32; (f) Chou PT, Chi Y. Phosphorescent dyes for organic light-emitting diodes. *Chem Eur J* 2007;13:380–95; (g) Li X, Minaev B, Ågren H, Tian H. Density functional theory study of photophysical properties of Iridium(III) complexes with Phenylisoquinoline and phenylpyridine ligands. *J Phys Chem C* 2011;115:20724–31.
- [3] Xiao L, Chen Z, Qu B, Luo J, Kong S, Gong Q, et al. Recent progresses on materials for electrophosphorescent organic light-emitting devices. *J Adv Mater* 2011;23:926–52.
- [4] Jeon WS, Park TJ, Kim SY, Podo R, Jang J, Kwon JH. Low roll-off efficiency green phosphorescent organic light-emitting devices with simple double emissive layer structure. *Appl Phys Lett* 2008;93:063303.
- [5] Meyer J, Hamwi S, Bülow T, Johannes HH, Riedl T, Kowalsky W. Highly efficient simplified organic light emitting diodes. *Appl Phys Lett* 2007;91:113506.
- [6] Liu ZW, Helander MG, Wang ZB, Lu ZH. Efficient bilayer phosphorescent organic light-emitting diodes: direct hole injection into triplet dopants. *Appl Phys Lett* 2009;94:113305.
- [7] Huang Q, Cui J, Yan H, Veinot JGC, Marks TJ. Small molecule organic light-emitting diodes can exhibit high performance without conventional hole transport layers. *Appl Phys Lett* 2002;81:3528.
- [8] Gao Y, Wang L, Zhang D, Duan L, Dong G, Qiu Y. Bright single-active layer small-molecular organic light-emitting diodes with a polytetrafluoroethylene barrier. *Appl Phys Lett* 2003;82:155.
- [9] Wang HF, Wang LD, Wu ZX, Zhang DQ, Qiao J, Qui Y, et al. Efficient single-active-layer organic light-emitting diodes with fluoropolymer buffer layers. *Appl Phys Lett* 2006;88:131113.
- [10] Tse SC, Tsung KK, So SK. Single-layer organic light-emitting diodes using naphthyl diamine. *Appl Phys Lett* 2007;90:213502.
- [11] Lai MY, Chen CH, Huang WS, Lin JT, Ke TH, Chen LY, et al. Benzimidazole/amine-based compounds capable of ambipolar transport for application in single-layer blue-emitting OLEDs and as hosts for phosphorescent emitters. *Angew Chem Int Ed* 2008;47:581–5.
- [12] Hung WY, Tsai TC, Ku SY, Chi LC, Wong KT. An ambipolar host material provides highly efficient saturated red PhOLEDs possessing simple device structures. *Phys Chem Chem Phys* 2008;10:5822–5.
- [13] Hung WY, Wang TC, Chiu HC, Chen HF, Wong KT. A spiro-configured ambipolar host material for impressively efficient single-layer green electrophosphorescent devices. *Phys Chem Chem Phys* 2010;12:10685–7.
- [14] Qiao X, Tao Y, Wang Q, Ma D, Yang C, Wang L, et al. Controlling charge balance and exciton recombination by bipolar host in single-layer organic light-emitting diodes. *J Appl Phys* 2010;108:034508.
- [15] Jeon WS, Park TJ, Kim KH, Podo R, Jang J, Kwon JH. High efficiency red phosphorescent organic light-emitting diodes with single layer structure. *Org Electron* 2010;11:179–83.
- [16] Erickson NC, Holmes RJ. Highly efficient, single-layer organic light-emitting devices based on a graded-composition emissive layer. *Appl Phys Lett* 2010;97:083308.
- [17] Chang HH, Tsai WS, Chang CP, Chen NP, Wong KT, Hung WY, et al. A new tricarbazole phosphine oxide bipolar host for efficient single-layer blue PhOLED. *Org Electron* 2011;12:2025–32.
- [18] You Y, Park SY. Phosphorescent iridium(III) complexes: toward high phosphorescence quantum efficiency through ligand control. *Dalton Trans* 2009:1267–82.
- [19] Beyer B, Ulbricht C, Escudero D, Friebe C, Winter A, Gonzalez L, et al. Phenyl-1H-[1,2,3]triazoles as new cyclometalating ligands for iridium(III) complexes. *Organometallics* 2009;28:5478–88.
- [20] Xia ZY, Xiao X, Su JH, Chang CS, Chen CH, Li DL, et al. Low driving voltage and efficient orange-red phosphorescent organic light-emitting devices based on a benzotriazole iridium complex. *Synth Met* 2009;159:1782–5.
- [21] Tomkute-Luksiene D, Malinauskas T, Stanisauskaite A, Getautis V, Kazlauskas K, Vitta P, et al. Efficient phosphorescent bis-cyclometalated iridium complex based on triazole-quinoline ligand. *J Photoch Photobio A* 2008;198:106–10.
- [22] Schaefer T, Murer P, Baudin G, Kocher M, Maike F, Allenbach S, et al. Electroluminescent metal complexes with benzotriazoles. *PCT Int Appl* 2008. WO 2008101842A1.
- [23] Malinauskas T, Daskeviciene M, Kazlauskas K, Su HC, Grazulevicius JV, Jursenas S, et al. Multifunctional red phosphorescent bis-cyclometalated iridium complexes based on 2-phenyl-1,2,3-benzotriazole ligand and carbazolyl moieties. *Tetrahedron* 2011;67:1852–61.
- [24] Cho MJ, Jin JI, Choi DH, Kim YM, Park YW, Ju BK. Phosphorescent, green-emitting Ir(III) complexes with carbazolyl-substituted 2-phenylpyridine ligands: effect of binding mode of the carbazole group on photoluminescence and electrophosphorescence. *Dyes Pigments* 2009;83:218–24.
- [25] Keruckas J, Lygaitis R, Simokaitiene J, Grazulevicius JV, Jankauskas V, Sini G. Influence of methoxy groups on the properties of 1,1-bis(4-aminophenyl)cyclohexane based arylamines: experimental and theoretical approach. *J Mater Chem* 2012;22:3015–27.
- [26] Kappaun S, Slugovc C, List EJW. Phosphorescent organic light-emitting devices: working principle and iridium based emitter materials. *Int J Mol Sci* 2008;9:1527–47.
- [27] Tsai MH, Hong YH, Chang CH, Su HC, Wu CC, Matoliukstyte A, et al. 3-(9-carbazolyl)carbazoles and 3,6-di(9-carbazolyl)carbazoles as effective host materials for efficient blue organic electrophosphorescence. *Adv Mater* 2007;19:862–6.
- [28] Zhang W, Wang Y, He Z, Mu L, Zou Y, Liang C, et al. Efficient electrophosphorescence based on 2-(9,9-diethylfluoren-2-yl)-5-trifluoromethylpyridine iridium complexes. *Synth Met* 2010;160:354–60.
- [29] Luka G, Stakhira P, Cherpak V, Volyniuk D, Hotra Z, Godlewski M, et al. The properties of tris (8-hydroxyquinoline) aluminum organic light emitting diode with undoped zinc oxide anode layer. *J Appl Phys* 2010;108:064518.
- [30] Chauhan G, Srivastava R, Tyagi P, Kumar A, Srivastava PC, Kamalasanan MN. Frequency dependent electrical transport properties of 4,4′-tris(N-3-methylphenyl-N-phenylamine)triphenylamine by impedance spectroscopy. *Synth Met* 2010;160:1422–6.